Room temperature oxidation kinetics of Si nanoparticles in air, determined by x-ray photoelectron spectroscopy

D.-Q. Yang, Jean-Numa Gillet, M. Meunier, and E. Sacher[a)]
Regroupement Québécois des Matériaux de Pointe and Département de Génie Physique, École Polytechnique Case Postale 6079, succursale Centre-Ville, Montréal, Québec H3C 3A7, Canada

(Received 28 June 2004; accepted 26 October 2004; published online 23 December 2004)

The air oxidation kinetics of low coverages of ~5 nm Si nanoparticles, deposited by pulsed excimer laser ablation (KrF, 248 nm) in He, have been characterized by x-ray photoelectron spectroscopy. A simple model, based on the evolution of the Si 2*p* spectral components during oxidation, has been developed to determine the nanoparticle oxide thickness. It is found that the short-term oxide thickness is greater, and the long-term room-temperature air oxidization rate of these nanoparticles is less, than those reported for bulk *a*-Si and *c*-Si. The results are also consistent with an earlier transmission electron microscope observation of the oxidation of larger Si particles at higher temperatures. The greater short-term oxide thickness may be attributed to surface defects on the prepared Si nanoparticles, and lower long-term oxidation rate is due to the nonlinear decrease of oxygen diffusion in spherical systems. © *2005 American Institute of Physics*.
[DOI: 10.1063/1.1835566]

INTRODUCTION

Nanostructured Si layers, including porous and nanostructured Si thin films, have been intensely studied over the last decade because of their potential applications in Si-based devices for optical communications and biosensors.[1,2] One of their interesting properties is the intense red photoluminescence (PL) of the nanostructured Si layer, which has been attributed to size-related quantum confinement effects[3] or oxidized defects related to the formation of the SiO_x/Si interface.[4,5] These effects have also explained the strong dependence of the PL on aging time in air. The instability of this PL in air is one of the most important factors hindering its application.

There is experimental evidence that the PL behavior, in both wet and dry oxygen (in air),[6–9] is related to the size of the nanoparticles,[6,7] the porosities of the thin films,[8,9] and the *x* value of the SiO_x layer.[10] Despite this, the origin of PL is still under debate.

While the oxidation kinetics of Si have been followed in pure oxygen, it has been more common to follow the kinetics in air, since that is what the Si is normally exposed to, and is of more interest to the PL applications community. Oxidation, in both media, follows the same log oxidation-log time plots,[11,12] although the rates are slightly greater in air and wet oxygen than in dry oxygen.

The deposition of nanostructured Si thin films, by laser ablation in rare gas ambients, has been accepted as one of most attractive methods of nanostructured thin films preparation[13–18] because it produces high purity Si nanoparticles. Such particles are ideal for studying surface oxidation and other gas phase reactions. The average particle dimensions, dependent on preparation parameters such as gas pressure, laser fluence, the distance between target and substrate, etc., can be controlled to give a typical diameter of ~5 nm.[6,9,15,18] The time-dependent behavior of the PL induced by the air oxidation of Si nanostructures has prompted us to explore the oxidization behavior of the Si particles because such a study will be useful in better understanding their oxidation-related PL properties, as well as in estimating the dimensions of any remaining Si in the nanoparticle core.

We previously used x-ray photoelectron spectroscopy (XPS) to study the oxidation of planar samples of bulk *a*-Si and *c*-Si under similar conditions.[19] Here, we use XPS to explore the oxidation parameters of nanoparticles, including oxide thickness, oxidation states, reaction rate because different oxidation states, from both Si nanoparticle shell and core, can easily be distinguished from the Si 2*p* spectrum; as well, the XPS information depth, three times the Si 2*p* attenuation length, is larger than dimensions of the Si nanoparticles considered here. We intentionally choose to study low coverages of Si nanoparticles on highly oriented pyrolytic graphite (HOPG), a relatively nonreactive surface, so as to provide the greatest free surface exposure to air, without screening effects, such as those found in the oxidation of porous Si,[20] without fear of substrate interaction.

EXPERIMENT

Si particles were deposited in a high vacuum laser ablation deposition system. The particles were produced by the KrF laser ablation (GSI Lumonics, Inc., PulseMaster™ PM-800, $\lambda = 248$ nm) of a Si target in high purity He. The laser operated at a repetition rate of 20 Hz, with a 20 ns full width at half maximum (FWHM). The laser radiation fluence at the Si target surface was ~2 J/cm^2, and the target was rotated at three revolutions per second. The base pressure in the preparation chamber was below 5×10^{-7} Torr and the He pressure was maintained at 2 Torr during Si nanoparticle deposition. The distance between target and substrate was 6 cm.

ZYA grade HOPG, 10 mm × 10 mm, 1 mm thick, was obtained from Advanced Ceramics and used as the deposi-

[a)]Electronic mail: edward.sacher@polymtl.ca

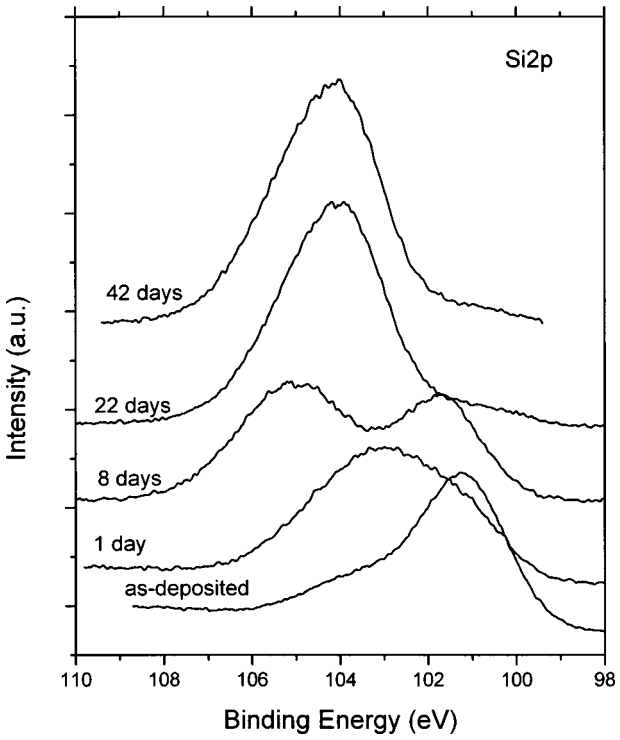

FIG. 1. XPS high resolution spectra of Si 2*p* for Si nanoparticles on HOPG, on exposure to air at room temperature.

tion substrate; its surface was parallel to the target surface. It was cleaved with adhesive tape just prior to each experiment and immediately inserted into the preparation chamber.

Ex situ XPS analysis was carried out in a VG ESCALAB 3 Mark II, using nonmonochromated Mg K_α x rays (1253.6 eV). The base pressure in the analysis chamber was less than 10^{-10} Torr. High-resolution spectra were obtained at a perpendicular take-off angle, using a pass energy of 20 and 0.05 eV steps. The instrument resolution was ~0.7 eV. After Shirley background removal, the component peaks were separated by the VG Avantage program; symmetrical Gaussian/Lorentzian peak shapes, and widths previously found by us for Si particles, were used. Air aging was carried out at 22±2 °C and 35% relative humidity. The peaks were calibrated to the HOPG C 1*s* peak at 284.6 eV.

RESULTS

The average coverage was estimated at 82%, using our previously described method,[21] with spherical nanoparticles, 5 nm in diameter.[6,9,16,18] XPS survey spectra of both as-deposited and long-term air oxidized Si nanoparticles films, with no HOPG present (not shown), indicate the presence of Si, O and, even after six months, less than 3 at. % contaminant C from the atmosphere. Thus, extensive C contamination does not occur in the present case.

Figure 1 shows the evolution of the Si 2*p* spectrum on oxidation. The envelope maximum shifts from ~101.3 eV for the as-deposited material (following ~30 min exposure during sample transfer) to ~105 eV after 42 days.

The chemical state of these Si nanoparticles changes with exposure to air, while the C 1*s* peak (not shown) shows no change during this period. This indicates that there is no

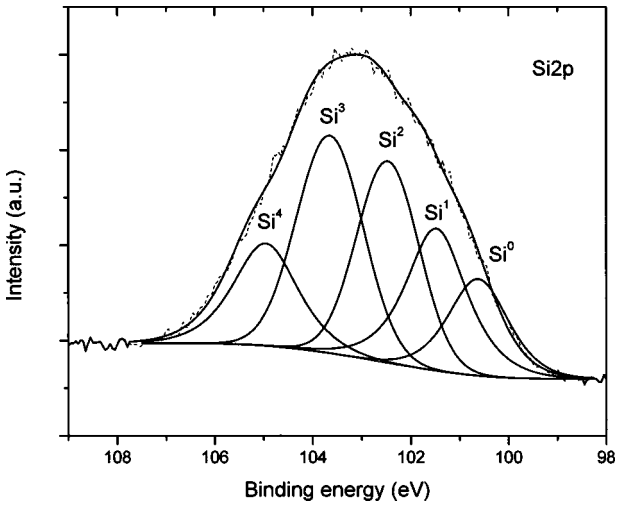

FIG. 2. Si 2*p* peak deconvolution for Si nanoparticles after 24 h exposure to air at room temperature.

reaction between the HOPG surface and the Si nanoparticles; further, the oxidation of Si nanoparticles does not affect the HOPG surface, despite the fact that the defect-related C 1*s* peaks in HOPG (285.6 and 286.5 eV) are quite sensitive to reaction.[22] We attribute the asymmetrical broadening and peak changes of the Si 2*p* spectrum in Fig. 1 to the commonly accepted superposition of five peaks, corresponding to the Si 2*p* core levels of Si^0 and each of the $Si–O_n$ basic bonding units in the a-SiO_x layer.[23–27] Based on our previous measurements on Si wafers on Ar sputtering and thermal oxidation, and in agreement with previous treatments of Si 2*p* spectral deconvolutions of SiO_x,[24,26] we have used a fixed peak FWHM value for all the component peaks. The Si 2*p* spectrum was thus separated into its component peaks, as shown in Fig. 2. The superscripts in the figure indicate the number of Si–O, as opposed to Si–Si, bonds, from Si^0 to Si^4; thus, Si^0, with Si bonded to four other Si, indicates bulk Si, while Si^4, with Si bonded to four O, indicates totally oxidized Si (i.e., SiO_2). All the component peaks are similarly shifted to slightly higher binding energies; the Si^0 peak is found at 100.5 eV, which is ~1.0 eV higher than that previously reported for bulk and thin film Si (~99.5 eV)[24–26] and for other Si nanoparticle studies,[27,28] although it is essentially identical to the 100.3 eV recently reported for Si nanoparticles on silver surfaces[29] and to our own *in situ* results on UHV-deposited, unoxidized Si nanoparticles.[30] The higher Si 2*p* binding energies in these cases may be attributed to initial- and final-state effects,[30,31] or related to an increase of the band gap[29] in the Si nanoparticles due to quantum size effects. The binding energies of the Si^1 and Si^3 chemical components, during air oxidation, are shown in Fig. 3. Because the energy separation of the various chemical components is constant, the Si^0, Si^2, and Si^4 components, which show similar trends, are omitted. The binding energies increase rapidly over the first 8 days of air oxidation, followed by stabilization and a slight decrease on further oxidation.

The evolution of the Si components, on oxidation in air, is seen in Fig. 4. With oxidation time, Si^0 and Si^1 are found to decrease rapidly, Si^3 and Si^4 to increase, and Si^2 to increase slightly. Both the Si oxidation products (the sum of

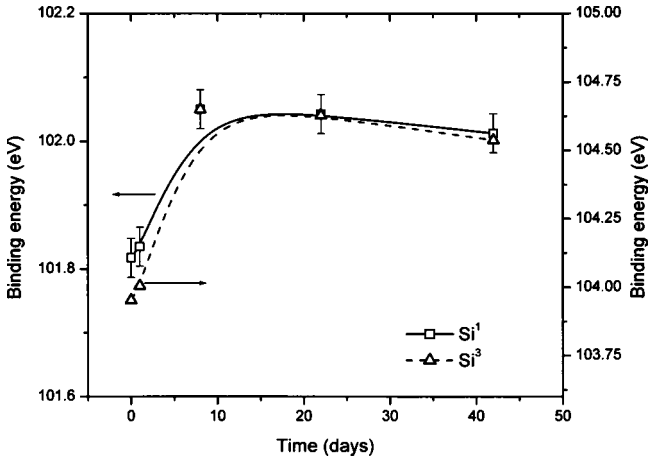

FIG. 3. Si^1 and Si^3 binding energies as a function of air oxidation time, obtained by Si 2*p* peak deconvolution.

Si^1, Si^2, Si^3, and Si^4) and the oxygen concentration (deduced from the O 1*s*: Si 2*p* peak intensity ratio) are plotted in Fig. 5, as a function of oxidation time. They are seen to vary in the same fashion but at different rates.

The magnitude of the Si^0–Si^4 separation varies with extent of oxidation, as found in Fig. 6. Its meaning will be discussed in the following section.

DISCUSSION

The oxidized Si 2*p* spectrum is composed of five chemical states, whose relative concentrations change with the extent of oxidation. In order to compare our results with those previously reported on bulk samples, we develop a simple model to describe the dependence of the relative concentration, as measured by XPS, on the oxide thickness.

Consider a nanoparticle made up of a spherical core and a uniform shell. The photoelectron signal intensity I of the core, with a radius r, surrounded by a shell with a thickness d can be expressed by the general formula[32]

$$I(\lambda,d,r)=\frac{\kappa(r/\lambda)d+\lambda}{d+\lambda}e^{-d/\lambda}\pi\lambda^3\{(r/\lambda)^2 + [(2r/\lambda+1)e^{-2r/\lambda}-1]/2\}, \quad (1)$$

where

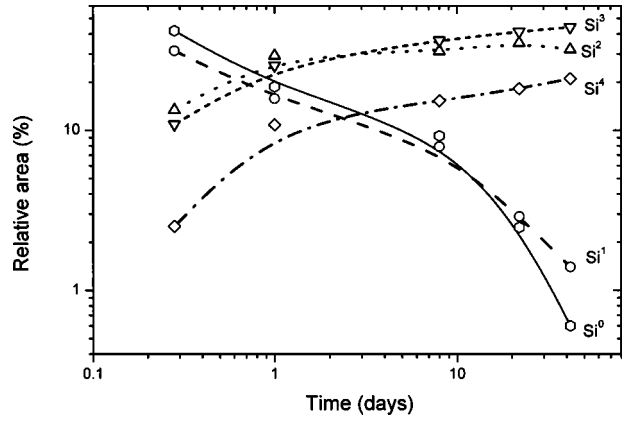

FIG. 4. Si peak components as a function of oxidation time in air at room temperature.

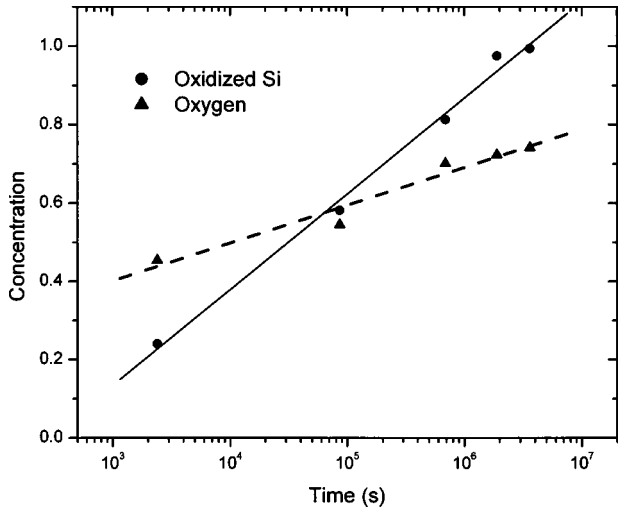

FIG. 5. Oxidation reaction kinetics of Si nanoparticles in air at room temperature.

$$\kappa(\rho)=\frac{\beta_1\rho^2+\beta_2\rho+1}{\beta_1\rho^2+\beta_3\rho+1}, \quad (2)$$

with $\rho=r/\lambda$, and the fitting constants $\beta_1=0.002\,89$, $\beta_2=0.051\,35$, and $\beta_3=0.459\,82$. For a partially oxidized spherical particle, r, in Eq. (1), denotes the unoxidized core radius and d, the oxidized shell thickness. Further, λ is the effective attenuation length in the core-shell nanoparticle, which depends on the photoelectron kinetic energy and is ~3.5 nm (λ_{SiO}) for SiO_2 and ~3.0 nm (λ_{Si}) for Si.[19] Although the complete mathematical demonstration of Eq. (1) is beyond the scope of this paper and will be given elsewhere,[32] we note that, when d is set to 0 in Eq. (1), the equation used by Wertheim and DiCenzo, for unoxidized spherical particles,[33] is reobtained.

The relative SiO_x concentration from the oxidized shell can then be computed as

$$C_{SiO}=\frac{I_{Shell}}{I_{Shell}+\mu I_{Core}}, \quad (3)$$

where $I_{Core}=I(\lambda_{Si},d,r)$ and $I_{Shell}=I(\lambda_{SiO},d=0,r+d)-I(\lambda_{SiO},d,r)$ are the respective core and shell intensities, computed from Eq. (1); $\mu=2.185$ is the ratio of the densities

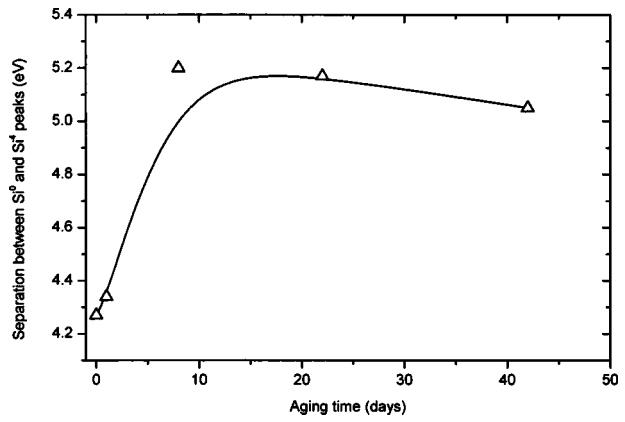

FIG. 6. The chemical shift between Si^0 and Si^4 states as a function of oxidation time.

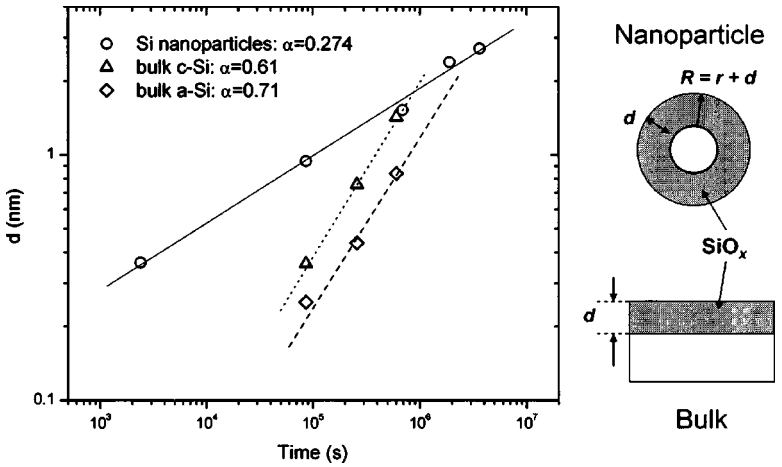

FIG. 7. Oxidation (thickness d) kinetics of Si nanoparticles in air at room temperature. Data on bulk material have been obtained from $I_{Si}=I_0e^{-d/\lambda_{SiO}}$.

of Si (4.96×10^{22} cm^{-3}) and SiO_2 (2.27×10^{22} cm^{-3}), which takes into account the density change from *c*-Si to *c*-SiO_2. It is not at all certain that the densities of the crystalline materials may be used here, so that C_{SiO} may, in fact, be slightly larger.

Further, from an expression based on the conservation of the number of Si atoms during oxidation,[32] we obtain the following relation between the core radius r and shell thickness d:

$$d_1^3 + 3r_1d_1^2 + 3r_1^2d_1 - \mu(1 - r_1^3) = 0, \tag{4}$$

where $d_1=d/r_0$ and $r_1=r/r_0$ are the respective d and r normalized by the initial core radius, $r_0=2.5$ nm. Note that the maximum value of d is $d_{max}=\mu^{1/3}\ r_0=3.24$ nm because $r=0$ in Eq. (4) when the nanoparticle is fully oxidized. The relationship $d=d(r)$ is then obtained by solving the third-order polynomial in Eq. (4), when r_1 varies from 0 to 1, taking the real root. Based on Eqs. (1)–(4) and the data in Fig. 4, we plot the oxidized Si thickness d, as a function of the oxidation time t, as shown in Fig. 7. For comparison, we also plot our previous oxide thickness data for bulk *a*-Si:H and *c*-Si.[19]. The oxide thickness variation with time clearly follows a *log–log* dependence, as previously reported for *c*-Si and *a*-Si oxidation in wet or dry O_2, at both room temperature and higher;[11,12,34–36] this indicates that the oxidation of Si nanoparticles follows an equation similar to that of bulk Si at all temperatures.

One should note that the oxidation rate for bulk *c*-Si is dependent on temperature, with higher temperatures giving higher oxidation rates.[11,12,35,36] However, there is an obviously difference in the case of Si nanoparticles: first, the initial oxidized thickness of the Si nanoparticles is greater than that of bulk Si, possibly due to a higher concentration Si surface free radicals that may easily react with the O_2 or H_2O present in air, both leading to the production of SiO_2: $Si+O_2\rightarrow SiO_2$ or $Si+2H_2O\rightarrow SiO_2+2H_2$. These reaction sites in the Si nanoparticles surface present no barrier to react with oxygen.[37] Second, the slope of the oxidation thickness with

TABLE I. A comparison of oxidation slopes.

Authors	*c*-Si and *a*-Si (bulk)	Larger Si particles (20–500 nm)	Si nanoparticles (6–33 nm)	Si nanoparticles (~5 nm)	References
Deal-Grove[a]	0.5				34
Blanc[a]	0.5–0.7				35
Vidal *et al.*[b]	0.7–0.9				36
Lu, Sacher, and Yelon[b]	0.61[c] 0.72[d]				19
Okada and Lijima[a]		Lower rate[e]			38
Hofmeister, Huisken, and Kohn[b]			Oxidation thickness decrease with particles size[f]		39
This work[b]				0.27	

[a]High temperature, dry oxidation, for thicker oxidation layers (>20 nm). The value can be as high as 0.9 for thin layers.
[b]Room temperature, dry oxidation, for thin oxidation layers.
[c]For *a*-Si:H, room temperature, wet oxidation, estimated from $I_{Si}=I_0e^{-d/\lambda_{SiO}}$, for thin oxidation layers.
[d]For *c*-Si, room temperature, wet oxidation, estimated from $I_{Si}=I_0e^{-d/\lambda_{SiO}}$, for thin oxidation layers. The slope is 0.9 for Ar^+-bombardment treated *c*-Si surface, as reported in Ref. 19, which may be caused by high density defects or dangling bonds in the treated Si surface.
[e]The specific value is not available, the results indicating that the oxidation rate of the particles decreased with decreasing particle dimensions.
[f]Room temperature air oxidation. No specific oxidation rate value is available.

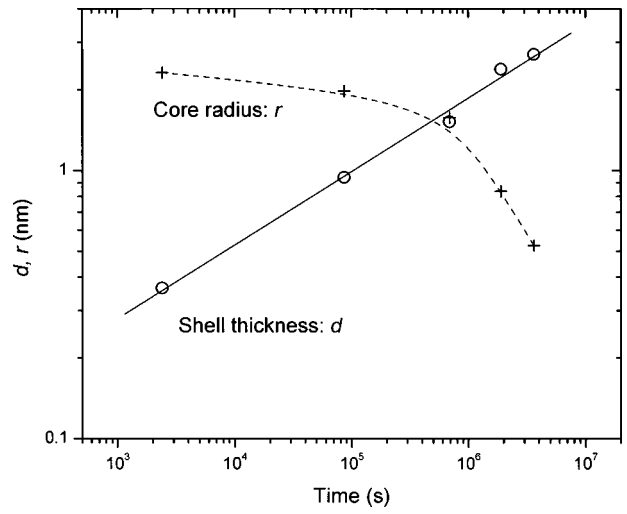

FIG. 8. Unoxidized core radius r and oxidized shell thickness d as a function of oxidation time, as determined using Eqs. (1)–(4) and data from Fig. 5.

time, in Fig. 7, is lower for nanoparticles. Although our results indicate the same oxidization reaction kinetics for both Si wafers and nanoparticles, we found that the slope α of oxidation in Si nanoparticles (see Fig. 7) is 0.27, which is smaller than that of *c*-Si and *a*-Si oxidations (α=0.4–0.9, Table I).[11,12,19,33–36] Because the slope is associated with the reaction rate and the diffusion coefficient of oxygen in Si, the smaller slope value in Si nanoparticles indicates weaker oxygen diffusion and reaction in nanoparticles. This conclusion is also consistent with the reported oxidation of 20–500 nm Si particles during high temperature oxidation,[38] and the room temperature oxidation of 6–33 nm Si nanoparticles, determined by transmission electron microscopy (TEM).[39] The slower oxidation rate for small Si particles in air, at high temperature, has been attributed to stress-induced suppression of the oxidization process.[38–40] However, the relative oxide concentration decreases nonlinearly with depth in the sphere,[41] and may also play an important role: the lower oxidation rate has been shown to depend on the depth below the surface of the nanoparticle and its curvature, decreasing with decreasing particle radius r, as the oxygen concentration driving the diffusion decreases, as may be seen from[41]

$$\frac{C}{C_0} = 1 + \frac{2a}{\pi r}\sum_{n=1}^{\infty}\frac{(-1)^n}{n}e^{-Dn^2\pi^2 t/a^2}\sin\frac{n\pi r}{a}, \tag{5}$$

where C is the time-dependent concentration of oxygen diffusing into the nanoparticles at a diffusion coefficient D, and C_0, the surface concentration; a is the initial oxidation shell thickness, r is the unoxidized Si core nanoparticle radius, and t is the time. Thus, the oxygen concentration decreases with depth [note that the sum term in Eq. (5) is negative], leading to the smaller slope in Fig. 7. In other words, the oxygen diffusion concentration decreases with the reciprocal of the core radius while, for bulk Si oxidation,[34] the decrease is linear with depth.

The difference between the measured oxygen and the Si oxide concentrations, in Fig. 5, indicates that oxygen diffusion is the rate-controlling process for nanoparticles, too. Further, the data in Fig. 5 and Eq. (3) permit the calculation of the radius of the unoxidized Si core of the particle with an initial diameter of 5 nm, and this is found, as a function of t, in Fig. 8. It is seen that the concentration of Si^0 extrapolates to zero in $\sim 10^7$ $\sim 10^8$ s, or around 4 months. This is substantially shorter than the time at which our system still shows photoluminescence, which is usually attributed to quantum confinement in Si nanocrystals. This question will be explored in a subsequent article.

The variation of the Si^0-Si^4 separation, in Fig. 6, is also found for ultra thin anodic silicon films during higher temperature annealing in oxygen.[42,43] Lau and Wu[42] have suggested that such changes in the peak separation are due to charging of the oxide film under the influence of the ionizing x rays, but Clark *et al.*[43] suggest that the shift may result from the occupancy of traps and defect levels by photogenerated holes, giving rise to a static charge, causing the Fermi level to move closer to the oxide conduction band edge. In this case, nonbridging oxygen, associated with incorporated OH and H_2O, are known to dominate in the defects as hole traps.

CONCLUSIONS

A simple model has been developed to determine the oxide thickness and oxidation rate of Si nanoparticles. The XPS determination of the oxidation and diffusion kinetics of supported Si nanoparticles, in air at room temperature, demonstrated that the oxidation and diffusion processes are similar those in bulk *c*-Si and *a*-Si for long term. However, the reaction rate and diffusion are lower than in these bulk materials, which is consistent with previous TEM measurements on larger Si particle oxidation at high temperatures.

ACKNOWLEDGMENT

The authors thank the Natural Sciences and Engineering Research Council of Canada for funding.

[1] L. Pavesi, L. Dal Negro, C. Mazzoleni, G. Franzo, and F. Priolo, Nature (London) **408**, 440 (2000).
[2] V. S.-Y. Lin, K. Motesharei, K. P. S. Dancil, M. J. Sailor, and M. R. Ghadiri, Science **278**, 840 (1997).
[3] L. T. Canham, Appl. Phys. Lett. **57**, 1046 (1990).
[4] S. M. Prokes and W. E. Carlos, J. Appl. Phys. **78**, 2671 (1992).
[5] L. N. Dinh, L. L. Chase, M. Balooch, L. J. Terminello, and F. Wooten, Appl. Phys. Lett. **65**, 3111 (1994).
[6] G. Ledoux, O. Guillois, D. Porterat, C. Reynaud, F. Huisken, B. Kohn, and V. Paillard, Phys. Rev. B **62**, 15942 (2000).
[7] D. P. Yu *et al.*, Phys. Rev. B **59**, R2498 (1999).
[8] M. V. Wolkin, J. Jorne, P. M. Fauchet, G. Allan, and C. Delerue, Phys. Rev. Lett. **82** , 197 (1999).
[9] A. V. Kabashin, J.-P Sylvestre, S. Patskovsky, and M. Meunier, J. Appl. Phys. **91**, 3248 (2002).
[10] I. Umezu, K.-I. Yoshida, N. Sakamoto, T. Murota, Y. Takashima, M. Inada, and A. Sugimura, J. Appl. Phys. **91**, 2009 (2002).
[11] D. R. Wolters and A. T. A. Zegers-van Duynhoven, Philos. Mag. B **55**, 669 (1987).
[12] E. A. Irene and R. Ghez, J. Electrochem. Soc. **124**, 1757 (1977).
[13] E. Werwa, A. A. Seraphin, L. A. Chiu, C. Zhou, and K. D. Kolenbrander, Appl. Phys. Lett. **64**, 1821 (1994).
[14] Y. Yamada, T. Orii, I. Umezu, S. Takeyama, and T. Yoshida, Jpn. J. Appl. Phys., Part 1 **35**, 1361 (1996).
[15] T. Makimura, Y. Kunii, and K. Murakami, Jpn. J. Appl. Phys., Part 1 **35**, 4780 (1996).
[16] T. Yoshida, S. Takeyama, Y. Yamada, and K. Mutoh, Appl. Phys. Lett. **68**,

1772 (1996).
[17]I. A. Movtchan, R. W. Dreyfus, W. Marine, M. Sentis, M. Autric, G. Le Lay, and N. Merk, Thin Solid Films **255**, 286 (1995).
[18]L. Patrone, D. Nelson, V. I. Safarov, M. Sentis, W. Marine, and S. Giorgio, J. Appl. Phys. **87**, 3829 (2000).
[19]Z. H. Lu, E. Sacher, and A. Yelon, Philos. Mag. B **58**, 385 (1988).
[20]D.-Q. Yang, M. Meunier, and E. Sacher (unpublished).
[21]D.-Q. Yang, K. N. Piyakis, and E. Sacher, Surf. Sci. **536**, 67 (2003).
[22]D.-Q. Yang and E. Sacher, Surf. Sci. **516**, 43 (2003).
[23]G. Hollinger and F. J. Himpsel, Phys. Rev. B **28**, 3651 (1983); W. Braun and H. Kuhlenbeck, Surf. Sci. **180**, 279 (1987).
[24]J. Finster, D. Schuler, and A. Meisel, Surf. Sci. **162**, 671 (1985).
[25]A. Fielman, Y.-N. Sun, and E. F. Farabaugh, J. Appl. Phys. **63**, 2149 (1988)
[26]F. G. Bell and L. Ley, Phys. Rev. B **37**, 8383 (1988).
[27]S. Hayashi, S. Tanimoto, and K. Yamanoto, J. Appl. Phys. **68**, 5300 (1990).
[28]S. T. Li, S. J. Silvers, and M. S. El-Shall, J. Phys. Chem. **101**, 1794 (1997).
[29]P. Mélinon *et al.*, J. Chem. Phys. **107**, 10278 (1997).
[30]D.-Q. Yang and E. Sacher (unpublished).
[31]D.-Q. Yang and E. Sacher, Appl. Surf. Sci. **195**, 187 (2002).
[32]J.-N. Gillet and M. Meunier (unpublished).
[33]G. K. Wertheim and S. B. DiCenzo, Phys. Rev. B **37**, 844 (1988).
[34]B. E. Deal and A. S. Grove, J. Appl. Phys. **36**, 3770 (1965).
[35]J. Blanc, Philos. Mag. B **55**, 685 (1987).
[36]R. Vidal, R. Koropecki, R. Arce, and J. Ferrón, J. Appl. Phys. **62**, 1054 (1987).
[37]K. Kato, T. Uda, and K. Terakura, Phys. Rev. Lett. **80**, 2000 (1998); T. Yasuda, N. Kumagai, M. Nishizawa, S. Yamasaki, H. Oheda, and K. Yamabe, Phys. Rev. B **67**, 195338 (2003).
[38]R. Okada and S. Lijima, Appl. Phys. Lett. **58**, 1662 (1991).
[39]H. Hofmeister, F. Huisken, and B. Kohn, Eur. Phys. J. D **9**, 137 (1999).
[40]J. Dalla Torre *et al.*, J. Appl. Phys. **92**, 1084 (2002); H. I. Liu, D. K. Biegelsen, F. Pone, N. Johnson, and R. Pease, Appl. Phys. Lett. **69**, 1232 (1996); H. I. Liu, D. K. Biegelsen, F. A. Ponce, N. M. Johnsen, and R. F. W. Pease, *ibid.* **64**, 1383 (1994).
[41]J. Crank, *The Mathematics of Diffusion*, 1st ed. (Oxford University Press, New York, 1956), Chap. 6.3.
[42]W. M. Lau, J. Appl. Phys. **67**, 1504 (1990); W. M. Lau and X.-W. Wu, Surf. Sci. **245**, 345 (1991).
[43]K. B. Clark, J. A. Bardwell, and J.-M. Barbeau, J. Appl. Phys. **76**, 3114 (1994).